Appl. Phys. B 75, 267–280 (2002)
DOI: 10.1007/s00340-002-0983-8

Applied Physics B
Lasers and Optics

Y. HE
B.J. ORR✉

Rapidly swept, continuous-wave cavity ringdown spectroscopy with optical heterodyne detection: single- and multi-wavelength sensing of gases

Department of Chemistry and Centre for Lasers & Applications, Macquarie University, Sydney, NSW 2109, Australia

Received: 16 May 2002/Revised version: 3 June 2002
Published online: 21 August 2002 • **© Springer-Verlag 2002**

ABSTRACT Spectroscopic sensing of gases can be performed with high sensitivity and photometric precision by cavity ringdown (CRD) absorption spectroscopy. Our cavity ringdown spectrometer incorporates continuous-wave (cw) tunable diode lasers, fibre-optic coupling and standard photonics and optical telecommunications components. It comprises a rapidly swept optical cavity in a single-ended optical heterodyne transmitter–receiver configuration, enabling optical absorption of gases to be recorded either as single-frequency scanned spectra or as simultaneous, multi-wavelength tailored spectra. By measuring weak near-infrared rovibrational spectra of carbon dioxide gas (CO_2), with high resolution in the vicinity of 1.53 μm, we have realised a noise-limited absorption sensitivity of 2.5×10^{-9} cm^{-1} Hz$^{-1/2}$. Analytical sensitivity limits (both actual and projected) and prospective gas-diagnostic applications are discussed. Our approach to cw-CRD spectroscopy offers high performance in a relatively simple, low-cost, compact instrument that is amenable to chemical analysis of trace gases in medical, agricultural, industrial and environmental situations.

PACS 07.07.Df; 33.20.-t; 42.62.Fi

1 Introduction

Cavity ringdown (CRD) laser absorption spectroscopy is now a mature, well-established technique [1–4], capable of measuring gas-phase molecular spectra with high sensitivity and photometric precision. The CRD approach employs coherent radiation, either pulsed [5] or continuous-wave (cw) [6, 7], to examine samples of gas contained in a high-finesse optical cavity. It continues to attract much activity and interest, in view of its potential for instrumental innovations and novel applications to trace gas detection and environmental sensing.

The very long effective optical path length achieved in a high-finesse cavity yields an enhancement factor of ($2 \times$ finesse$/\pi$) and provides an intrinsic advantage for CRD spectroscopy [1–4]. Moreover, the experimental quantity measured is a ringdown decay time τ rather than optical power or energy. The corresponding first-order rate constant, τ^{-1}, is plotted against laser wavelength or frequency to generate a CRD spectrum. Such spectra can therefore be recorded with extremely low absorbances and with little or no sensitivity to amplitude fluctuations of the tunable coherent radiation employed. In addition, when cw or long-pulse lasers are used, the flux of intracavity radiation can be built up to facilitate use of relatively low-power coherent light, such as tunable diode laser (TDL) sources.

The introduction of CRD spectroscopy with pulsed light sources [5] has been taken up by many research groups [1–4] – including our own, in the context of narrowband pulsed optical parametric oscillator (OPO) devices [8–10]. CRD spectroscopy performed with cw lasers has some advantages relative to its pulsed-laser counterpart, in that higher spectroscopic resolution can be attained and it is possible to use inexpensive, compact single-mode TDL sources. Compared to a typical pulsed laser, the spatial beam profile of such a TDL is generally superior, which helps to couple the laser light into the ringdown cavity. However, it is necessary in the cw-CRD approach to interrupt the passage of light through the ringdown cavity, as is illustrated conceptually in Fig. 1. This generally entails at least one of the following three operational strategies:

(a) the use of a fast optical switch, either acousto-optic (AO) or electro-optic (EO);
(b) the use of rapid electronic modulation of either the frequency or amplitude of the cw light;
(c) the variation of the length, and hence optical resonance frequency, of the ringdown cavity.

The earliest implementations of cw-CRD spectroscopy [6, 7] and its more recent refinements [11–13] have depended primarily on strategy (a), combined in some cases with (b) and (c), to ensure that the optical cavity and the light are in resonance. However, AO and EO switches tend to be expensive, cumbersome and limited in their spectral range, so that there is some practical advantage in eliminating them in applications where compactness, portability, cost and wavelength range are considered. Reliable, reproducible electronic control of TDL amplitude and frequency is not at all straightforward, particularly for high-resolution cw-CRD-spectroscopic applications. The preferred approach in our laboratory [9, 14, 15] and elsewhere [16] has therefore been to implement strategy (c), thereby avoiding the inherent complexity and expense of an AO or EO switch.

✉ Fax: +61-2/9850-8313, E-mail: brian.orr@mq.edu.au

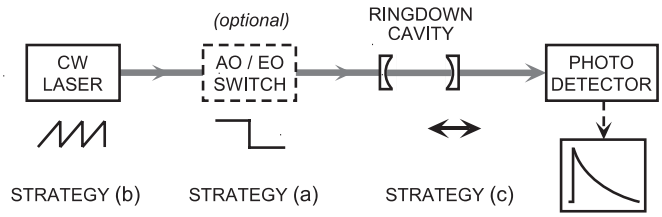

FIGURE 1 Schematic of a generalised cw-CRD spectrometer, comprising a cw laser (or other cw coherent light source), an optional acousto-optic (AO) or electro-optic (EO) switch, a high-finesse optical ringdown cavity, and a fast, low-noise photodetector to monitor light transmitted by the cavity. This is linked to suitable electronic instruments to display, record and process ringdown decay curves. Three possible operational strategies are depicted, comprising: (a) interruption of the incident light by the fast AO or EO switch; (b) some form of electronic modulation (not necessarily saw-tooth) of either the frequency or amplitude of the cw laser; and (c) rapid variation of the length of the ringdown cavity

In our approach [9, 14, 15], we use a piezoelectric translator (PZT) to rapidly sweep the length of the optical cavity through resonance with narrowband cw TDL radiation. This proves to be a straightforward way to facilitate growth and subsequent ringdown decay of optical energy in the cavity and yields absorption spectra with high sensitivity and with minimal instrumental complexity and cost. In an alternative approach [16], the ringdown cavity length is rapidly displaced in a single step after the wavelength of the cw laser has reached a cavity resonance and optical energy has built up in the cavity.

A further distinctive refinement of our rapidly swept cw-CRD spectroscopic technique comprises an optical-heterodyne-detected (OHD) approach [14, 15], as depicted in Fig. 2. Our approach is intrinsically simpler than other OHD variants of cw-CRD spectroscopy [11–13] that employ at least one active EO or AO modulator to generate OHD sidebands. Figure 2 is configured to demonstrate one of the principal advantages of our OHD cw-CRD technique, namely, that it enables "single-ended" detection with both the optical transmitter and receiver naturally collocated in a single console that can be widely separated from the rapidly swept ringdown cavity module.

The conventional way to detect a CRD signal is via the forward-propagating ringdown light field, $\boldsymbol{E}_\mathrm{F}\exp(-t/2\tau)$, using a photodetector (not shown explicitly in Fig. 2) to extract the ringdown time constant τ from the exponentially decaying temporal envelope of its intensity, $|\boldsymbol{E}_\mathrm{F}|^2\exp(-t/\tau)$. In our OHD cw-CRD technique, we look instead at the backward-propagating light actively reflected off the rapidly swept cavity. This may be envisaged as a heterodyne beat signal between the directly reflected portion, $\boldsymbol{E}_\mathrm{I}$, of the incident laser light field, $\boldsymbol{E}_\mathrm{L}$, and the backward-propagating ringdown light field, $\boldsymbol{E}_\mathrm{B}\exp(-t/2\tau)$ – virtually identical to the above forward-propagating light that is usually detected. The moving mirror of a rapidly swept cavity Doppler-shifts the frequency of the optical fields $\boldsymbol{E}_\mathrm{F}$ and $\boldsymbol{E}_\mathrm{B}$, as is further explained in Sect. 2.2. The outcome is an OHD signal $\langle S\rangle$ collected at photodetector PD_1, of the form:

$$\begin{aligned}\langle S\rangle &\propto |\boldsymbol{E}_\mathrm{I}+\boldsymbol{E}_\mathrm{B}\exp(-t/2\tau)|^2\\ &= |\boldsymbol{E}_\mathrm{I}|^2+|\boldsymbol{E}_\mathrm{B}|^2\exp(-t/\tau)\\ &\quad+2\,\mathrm{Re}\left(\boldsymbol{E}_\mathrm{I}^*\times\boldsymbol{E}_\mathrm{B}\right)\exp(-t/2\tau),\end{aligned}\tag{1}$$

where relatively rapid time dependencies at optical frequencies are implicitly included in optical fields such as $\boldsymbol{E}_\mathrm{L}$, $\boldsymbol{E}_\mathrm{I}$, $\boldsymbol{E}_\mathrm{F}$ and $\boldsymbol{E}_\mathrm{B}$, but the slow ringdown decay of the temporal envelope of $\boldsymbol{E}_\mathrm{F}$ and $\boldsymbol{E}_\mathrm{B}$ during the cavity sweep is treated explicitly. Although PD_1 averages the high-frequency time dependence of optical fields $\boldsymbol{E}_\mathrm{I}$ and $\boldsymbol{E}_\mathrm{B}$, the distribution of Doppler-induced frequency shifts between them allows their cross term to appear as an OHD signal.

This optical heterodyne cross term comprises the product of $(\boldsymbol{E}_\mathrm{I}^*\times\boldsymbol{E}_\mathrm{B})$ and a slowly varying exponential decay factor $\exp(-t/2\tau)$ that depends on the cavity ringdown time τ. The term in $|\boldsymbol{E}_\mathbf{B}|^2$ is comparable to the direct cw-CRD signal in $|\boldsymbol{E}_\mathrm{F}|^2$ that is conventionally monitored in the forward-propagating direction, as in our original direct (non-OHD) cw-CRD method [14]. A significant amplification factor arises in the OHD case because the amplitude of the optical field $\boldsymbol{E}_\mathrm{I}$ is much greater than that of $\boldsymbol{E}_\mathrm{B}$ or $\boldsymbol{E}_\mathrm{F}$, by which it is multiplied. Detection sensitivity can be further enhanced by the fact that the temporal envelope of the OHD signal ($\mathrm{e}^{-t/2\tau}$) decays twice as slowly as that of the direct (forward-propagating) ringdown signal ($\mathrm{e}^{-t/\tau}$); this is because the dependence on the ringdown field is linear in the former (OHD) case, whereas it is quadratic in the latter (non-OHD) case. Moreover, the higher frequency domain of the OHD signal allows a high-pass filter to be used to reduce low-frequency technical noise.

In Sect. 4, we introduce novel variants of our rapidly swept OHD cw-CRD spectroscopic technique that enable simultaneous, multi-wavelength detection. Before that, in Sects. 2 and 3, details of the basic single-wavelength OHD and direct (non-OHD) forms of rapidly swept cw-CRD spectroscopy [9, 14, 15] are surveyed, including innovative technological refinements not previously reported.

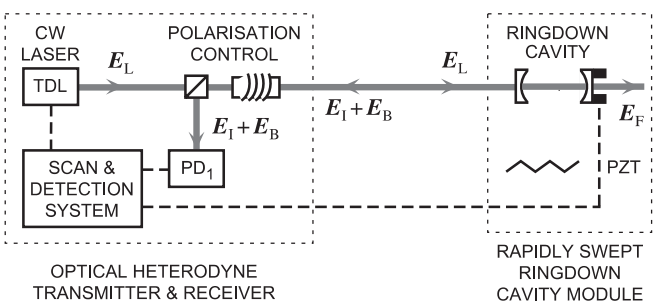

FIGURE 2 Schematic of the optical-heterodyne-detected (OHD) form of swept-cavity cw-CRD spectrometer. This shows the highly advantageous "single-ended" detection configuration, with both optical transmitter and receiver collocated in a single console that can be widely separated from the rapidly swept ringdown cavity module. $\boldsymbol{E}_\mathrm{L}$, $\boldsymbol{E}_\mathrm{I}$, $\boldsymbol{E}_\mathrm{F}$, and $\boldsymbol{E}_\mathrm{B}$ denote electric field amplitudes for light propagating at various points in the apparatus. TDL, tunable diode laser; PD, photodetector; PZT, piezoelectric translator

2 Single-wavelength rapidly swept cw-CRD methodology

2.1 *Basic instrumentation*

Details of the basic single-wavelength instrumentation used for our rapidly swept cw-CRD spectroscopic technique, either direct or OHD, have been presented elsewhere [9, 14, 15]. A typical set-up is described below, with

reference to Fig. 2. The cw laser is an external-cavity TDL (New Focus model 6262 with model 6200 controller, ∼ 5-mW single-mode output; continuously tunable over a wavelength range 1.50–1.59 μm with ∼ 1-MHz optical bandwidth). To record CRD spectra, the TDL wavelength is step-scanned slowly, averaging a suitable number of ringdown curves at each step. The components labelled "polarisation control" comprise two Faraday-rotator optical isolators (Optics for Research model IO-4-IR2-HP) with overall 80 dB attenuation; these include a polarising beam splitter that directs the backward-propagating light fields $\boldsymbol{E}_{\mathrm{I}}$ and $\boldsymbol{E}_{\mathrm{B}}$ to the OHD photodetector PD_1, making efficient use of available laser power for OHD measurements. Photodetector PD_1 comprises an InGaAs photodiode with matching low-noise preamplifier (New Focus model 1811, 125-MHz bandwidth); a second identical photodetector (PD_2, not shown explicitly in Fig. 2) is used to monitor the direct, forward-propagating CRD signal (depending on $\boldsymbol{E}_{\mathrm{F}}$). The ringdown cavity comprises two concave mirrors (Newport model 10CV00SR.70F, > 99.96% reflectivity, −1-m radius, typically 45 cm apart) mounted in an evacuable optical cell fitted with electronic manometers. A cylindrical low-voltage PZT (Piezotechnik model HPSt 150/20), driven by a ramp with approximately 7-V amplitude, allows the ringdown cavity length to be swept with an amplitude of approximately 1.0 μm (slightly more than one free spectral range) at frequencies up to approximately 1 kHz. The TDL beam is mode-matched to the ringdown cavity by a lens of 50-cm focal length. The section labelled "scan and detection system" in Fig. 2 comprises various electronic instruments: the current, temperature and wavelength-scan control unit for the TDL (New Focus model 6200); low-noise amplifiers that are incorporated in photodetectors PD_1 and PD_2; a digital oscilloscope (Tektronix model TDS3054, 500-MHz bandwidth, 9-bit vertical resolution); a PZT sweep-voltage controller (Hewlett Packard model 3310A); a computer with an IEEE-488 interface.

A synchronous gate selects the portion of signal output from PD_1 and/or PD_2 around the midpoint of each positive-going PZT sweep, where the velocity of the cavity mirror is constant (typically $\sim 1\ \mathrm{mm\,s^{-1}}$). The digital oscilloscope is level-triggered by the ringdown signal, since cavity resonances occur at points in the sweep cycle that vary as the input TDL wavelength is scanned. Successive ringdown curves are collected at a rate of approximately 500 Hz and averaged in the oscilloscope, with a dead time of approximately 0.1 s, during which a ringdown time τ is extracted from the averaged waveform (typically over the range $5 < t < 50\ \mu\mathrm{s}$) and the TDL wavelength is incremented (in steps of approximately 0.01 nm for a coarse scan or approximately 0.4 pm for a fine scan). It is therefore feasible to make an automated 256-sweep average of each CRD-spectroscopic data point within a time interval of approximately 0.6 s.

2.2 *Rapidly swept cw-CRD waveforms*

Two simultaneously recorded rapidly swept cw-CRD waveforms are presented in Fig. 3. Each is recorded in a single PZT-driven sweep of the length of the ringdown cavity, without any signal averaging. Figure 3a shows the direct, forward-propagating signal (detected by PD_2), while Fig. 3b corresponds to the backward-propagating OHD signal (detected by PD_1). The oscillatory behaviour of each of these waveforms is understood in terms of the dynamic response of cw coherent radiation to an optical cavity whose length is swept rapidly and continuously by means of a PZT.

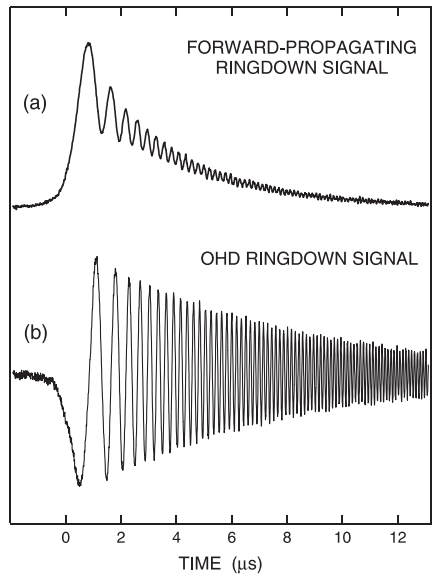

FIGURE 3 Simultaneously recorded, rapidly swept cw-CRD waveforms: (a) observed directly, as a forward-propagating signal; and (b) observed as a backward-propagating OHD signal (detected by PD_1, as depicted in Fig. 2). Each waveform is recorded in a single PZT-driven sweep of the length of the ringdown cavity, without any signal averaging. The oscillatory behaviour of each of these waveforms is understood in terms of the dynamic response of cw coherent radiation to an optical cavity whose length is swept rapidly and continuously by means of a PZT. The exact resonance point between the rapidly swept cavity and the laser wavelength occurs at sweep time $t = 0$ on the abscissa

A tiny cavity mirror displacement (∼ 1 nm) suffices to shift such ringdown cavities on and off resonance, as they have very high finesse (typically $\sim 10^4$). Optical energy is built up and stored in the cavity as any of its modes moves into resonance with the laser wavelength, and the cavity then transmits more light. The input light is effectively blocked by the highly reflective cavity mirrors once the swept cavity moves off resonance with the narrowband incident laser light; the light stored in the cavity during the build-up period then decays gradually with a ringdown time constant τ that depends on the mirror reflectivity and the absorption of the optical medium inside the cavity.

An essential feature of our rapidly swept CRD approach is the effect of Doppler-type frequency shifts $\Delta\nu_j$ that accumulate with each reflection of intracavity radiation from a continuously moving mirror:

$$\Delta\nu_j = (\nu_{j+1} - \nu_j) = \nu_j(2v/c), \tag{2}$$

where ν_j is the frequency of light on its jth round trip in the cavity, v is the mirror velocity, and c is the speed of light. A distribution of intracavity optical fields is therefore generated during multiple passes of the rapidly swept cavity. At any instant in the cavity sweep cycle, the frequency distribution of these intracavity optical field components is relatively narrow (within the convolution of the optical bandwidth of the

coherent light source and the transmission bandwidth of the ringdown cavity). The spread of the distribution remains stable after the cavity is moved off resonance, while its centre frequency follows the continuing change of the cavity resonance frequency as the position of the cavity mirrors is varied.

Oscillatory cavity ringdown signals, as in Fig. 3, arise as the accumulated Doppler-shifted fields in the cavity interfere with each other and with the (unshifted) incident radiation. For amplitudes of mirror travel and ringdown times that are typical in our swept-cavity cw-CRD experiments, the resultant frequency shifts span the range 0–10 MHz (0–0.0003 cm^{-1}). The oscillations become increasingly frequent as the sweep time t increases, because the frequency shift increases with the number of passes. Such effects are absent in more conventional cw-CRD approaches in which the ringdown-cavity length and laser frequency are fixed.

The temporal profile of the forward-transmitted cw-CRD light intensity [9, 14, 15] is seen in Fig. 3a to be asymmetric, with a rapid build-up phase (peaking just after the exact resonance point at $t = 0$ on the abscissa between the cavity and the laser wavelength), followed by a slowly decaying tail that exhibits characteristic ringing due to interference of the multiply reflected intracavity light. The corresponding oscillatory OHD waveform in Fig. 3b contains information about the amplitudes and relative phase of the optical fields $\boldsymbol{E}_{\mathrm{I}}$ and $\boldsymbol{E}_{\mathrm{B}}$ that are monitored by PD_1 and (as will be demonstrated in Sect. 3.2 below) its exponentially decaying envelope gives a reliable measure of 2τ.

We have performed numerical simulations by superposing multiply reflected cw laser radiation in a rapidly swept optical cavity, assuming that the incident laser radiation is monochromatic. The phase and amplitude of the multiply reflected beams are calculated at each round trip by taking account of the Doppler frequency shifts, slight changes in the intracavity round-trip time, and the attenuation of amplitude associated with the continuously varying transmission characteristics of a rapidly swept optical cavity. Parameters used to simulate the properties of the empty cavity are: wavelength, $\lambda = 1.530\,\mu\mathrm{m}$; cavity length $L = 0.453\,\mathrm{m}$ (at rest); free spectral range, FSR = 331 MHz; ringdown time, $\tau = 3.57\,\mu\mathrm{s}$ (best fit to experiment); time to sweep through 1 FSR = 0.335 ms; effective mirror reflectivity (consistent with τ), $R = 0.9996$; and finesse $= 7.42 \times 10^3$. The single-sweep observations shown in Fig. 3a and b and Fig. 4a and b are compared with simulations in Fig. 4c and d, and corresponding residual plots in Fig. 4e and f. There is good qualitative agreement between the observed and stimulated curves; significant but subtle differences are discussed below.

The differences between observed and simulated signals are most dramatic for backward-propagating OHD cw-CRD, as shown in Fig. 4b, d and f, and most pronounced at a sweep delay t above approximately 6 μs. Here, just above $t = 6\,\mu\mathrm{s}$, the two sets of oscillations in Fig. 4b and d shift out of step, resulting in a Moiré-type interference pattern when they are superimposed. The pronounced interference effect shown in Fig. 4f and less clearly in Fig. 4e is most likely due to a shift in the laser frequency, within the limits of its short-term stability rating of approximately 1 MHz. An irregularity in the cavity scan rate is another possible explanation, but less likely. Irregularities within the ringdown

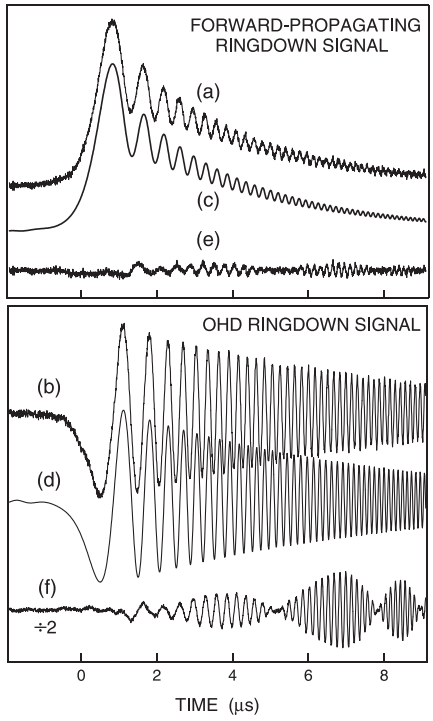

FIGURE 4 Observed (a, b) rapidly swept cw-CRD waveforms (as in Fig. 3), compared with corresponding simulations (c, d) and residuals (e, f) for direct, forward-propagating (a, c, e) and OHD backward-propagating (b, d, f) modes of detection, respectively. The residual plot (f), halved in amplitude relative to waveforms (b) and (d), indicates that shifts in laser frequency (or possibly cavity-sweep linearity) introduce pronounced phase differences between the observed and simulated waveforms at and above sweep times $t \approx 6\,\mu\mathrm{s}$

time, such as those shown in Fig. 4e and f, are typical but irreproducible from one cavity sweep to the next. However, they do not detract directly from our ability to determine an accurate ringdown time τ from the *envelope* of the waveform, rather than from the *oscillations*, as we shall demonstrate in Sect. 3.2 below, where a demodulating logarithmic amplifier is used. Nevertheless, the laser frequency needs to be stable on the timescale of the build-up of light in the cavity, since a substantial shift in laser frequency will lead to secondary build-up processes, causing the envelope of backward- (OHD) and forward-propagating waveforms to be weakly modulated as a result of the frequency shift. In the present case, the resonance frequency of the cavity is swept at a rate of $1.0\,\mathrm{MHz}\,\mu\mathrm{s}^{-1}$ with a finite cavity bandpass (FSR/finesse; ~ 45 kHz; $\sim 1.5 \times 10^{-6}\,\mathrm{cm}^{-1}$), so that the short-term frequency stability of the laser needs to be approximately 100 kHz, say. Therefore, we anticipate that a more stable laser frequency could further improve the detection sensitivity.

It is interesting to note that weak oscillatory behaviour is predicted in the range of t between 0 and $-2\,\mu\mathrm{s}$ in Fig. 4d, well before the leading edge of the build-up phase; it is consistent with the ringdown cavity's finite bandpass (~ 45 kHz – see above). This effect is not clearly observed in the corresponding part of Fig. 4b.

The intracavity optical interference effects that produce such oscillatory waveforms are by no means new. Time-response effects in a Fabry–Pérot interferometer cavity, par-

alleling our original direct cw-CRD simulation [14] and that in Fig. 4a, have previously been characterised [16–20] under conditions in which the rapidly swept variable is either the optical cavity length (with fixed incident frequency) [16, 17, 19, 20] or the incident optical frequency (with fixed cavity length) [17, 20]. Likewise, OHD cw-CRD waveforms such as in Figs. 3b and 4b, previously reported by us [9, 15], are consistent with other earlier investigations [20, 21]. Hall and co-workers [21] first observed and modelled a similar waveform as "cavity beating decay" by using a fixed-length cavity to reflect laser light with its frequency rapidly swept through the cavity resonance. In a comprehensive study of the dynamic response of a Fabry–Pérot interferometer [20], Byer and co-workers also observe and predict waveforms similar to our OHD signals in Figs. 3b and 4b.

2.3 *OHD cw-CRD spectra*

To demonstrate the applicability of our cw-CRD technique, we have previously published [9, 14, 15] finely resolved rovibrational absorption spectra of carbon dioxide (CO_2) gas in the vicinity of 1.52–1.55 μm (6450–6570 cm^{-1}). The ultimate test of our OHD cw-CRD technique is provided by the spectrum in the region of the Q-branch of the 6538-cm^{-1} $(11^12)_{II}$–(00^00) combination band [22] of CO_2, reproduced in Fig. 5a. This comprises a plot of the CRD absorption coefficient (units: 10^{-6} cm^{-1}; linearly dependent on τ^{-1}) against the continuously scanned TDL frequency (cm^{-1}), recorded with CO_2 pressure $P = 50$ mbar and $T = 296$ K. Spectroscopic data points are recorded at TDL frequency intervals of approximately 0.0017 cm^{-1}, each averaged over 256 cavity sweeps. The observed linewidths (0.018 cm^{-1} FWHM) are determined by a combination of Doppler and pressure broadening. In Fig. 5a, prominent features of the $(11^12)_{II}$ – (00^00) Q-branch (band origin = 6537.959 cm^{-1}) are labelled with corresponding rotational quantum numbers $J = 2$–14. We have previously identified the other features (A–G) [9].

The HITRAN'96 program [22] provides reliable assignments [9, 15] of the three stronger additional peaks (A, B, F) in Fig. 5a to rovibrational lines of $^{12}CO_2$, as follows:

Peak A: 6538.01 cm^{-1} (obs.) $(40^01)_I$ – $(10^00)_I$ R(6)
6538.02 cm^{-1} [22]
Peak B: 6537.99 cm^{-1} (obs.) $(31^11)_I$ – (01^10) R(1)
6537.99 cm^{-1} [22]
Peak F: 6537.29 cm^{-1} (obs.) $(30^01)_I$ – (00^00) R(50)
6537.29 cm^{-1} [22] .

A simulation of the observed spectrum (derived from the HITRAN'96 database [22]) is also shown in Fig. 5b, inverted and offset downwards by 1.0×10^{-6} cm^{-1} and accompanied by a residual (experiment – simulation) plot in Fig. 5c (offset downwards by 0.5×10^{-6} cm^{-1}). The abscissa is referenced (more accurately than before [9, 15]) to the HITRAN'96-predicted frequencies [22]. The agreement is generally excellent, with discrepancies suggesting minor deficiencies of HITRAN'96 (e.g. in relative intensities of different rovibrational absorption bands, some of them temperature-sensitive hot bands) and in experimental conditions (e.g. minor nonlinearities in the TDL wavelength scan).

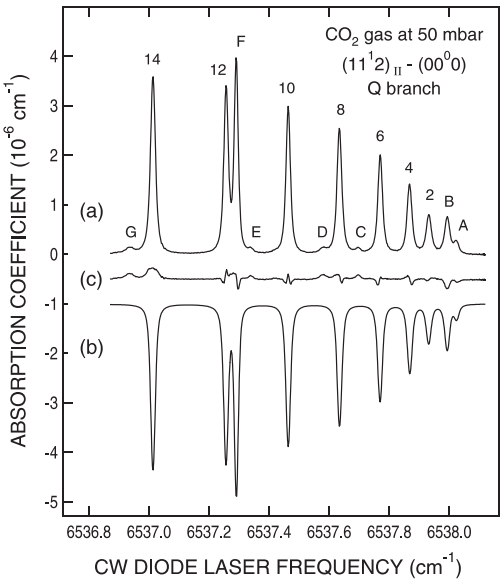

FIGURE 5 Rovibrational absorption spectrum of carbon dioxide (CO_2) gas in the region of its Q-branch of the 6538-cm^{-1} $(11^12)_{II}$ – (00^00) combination band. Part (a) is recorded by the rapidly swept cw-CRD technique with a CO_2 pressure $P = 50$ mbar and $T = 296$ K; it is averaged over 256 cavity sweeps. Assignments are discussed in the text. The observed noise-limited sensitivity is estimated to be 2.5×10^{-9} cm^{-1} $Hz^{-1/2}$. Part (b) is a simulated spectrum (derived from the HITRAN'96 database [22]), inverted and offset downwards by 1.0×10^{-6} cm^{-1}. Part (c) is a residual (experiment – simulation) plot, offset downwards by 0.5×10^{-6} cm^{-1}

Observations have not previously been made of the four other much weaker features (C, D, E and G) in Fig. 5a. From available spectroscopic information [22, 23], we have previously made tentative assignments of these hitherto unidentified features [9], attributing them to specific sources such as isotopic species of CO_2 (e.g. $^{13}CO_2$) and/or ultra-weak hot bands. It is now possible that two of the features are more appropriately assignable via HITRAN'96 [22] to traces of water vapour (H_2O), rather than to CO_2 itself [9], as follows:

Peak D: 6537.58 cm^{-1} (obs.) $H_2O\ 021^- \leftarrow 000\ 7_{1,6} \leftarrow 8_{3,5}$
6537.58 cm^{-1} [22]
Peak G: 6536.94 cm^{-1} (obs.) $H_2O\ 120^- \leftarrow 000\ 7_{3,4} \leftarrow 8_{4,5}$
6536.95 cm^{-1} [22]

2.4 *Noise-limited sensitivity, detection limits and dynamic range*

From the observed baseline noise level in Fig. 5a, we estimate that the noise-limited sensitivity for absorption detection is 3×10^{-9} cm^{-1}. Taking account of our data acquisition time of approximately 0.6 s per data point (based on a 256-sweep average), this corresponds to a normalised minimum detectable absorption loss of 2.5×10^{-9} cm^{-1} $Hz^{-1/2}$.

This sensitivity compares favourably with that of many other forms of cw-CRD spectroscopy [3, 4, 6, 7, 11–13, 16], generally obtained with more elaborate instrumentation. However, they still fall short of the state of the art in this field. In a recent cw-CRD spectroscopic study of $^{12}CO_2$ and $^{13}CO_2$ gas mixtures at approximately 6262 cm^{-1} (∼ 1.60 μm) [24], Paldus, Zare and colleagues report a minimum detectable

absorption loss of $3.2 \times 10^{-11}\,\mathrm{cm}^{-1}\,\mathrm{Hz}^{-1/2}$ – two orders of magnitude better than our result. They used an advanced, thermally regulated cw-CRD instrument incorporating a commercial external-cavity TDL, a reference étalon for wavelength calibration, an AO modulator, a PZT-scanned three-mirror ring cavity ($R = 0.99996$, round-trip path length = 42 cm), a fast InGaAs photodetector, a 16-bit digitiser, and a triggering/tracking circuit cycling at 1 kHz and linked to the AOM, PZT and photodetector. Even higher sensitivity ($1 \times 10^{-14}\,\mathrm{cm}^{-1}\,\mathrm{Hz}^{-1/2}$) has been achieved by Hall and colleagues [25], using advanced noise-immune OHD FM-spectroscopic techniques. There is a major trade-off between sensitivity and instrumental refinements such as laser- and cavity-stabilisation, mirror reflectivity, use of EO and/or AO modulators, and extent of feedback control measures. Our main objective has been to develop a relatively simple, compact, economical cw-CRD spectroscopic system, rather than to extend the limits of detection sensitivity.

We estimate that our experimental system has a dynamic range (over which linear CRD signal detection is possible, relative to the noise level) of at least 35 dB (i.e. a factor of 3000). This dynamic range depends on a number of factors, including the noise level and the linear amplification range of the photodetector and its preamplifier. The latter factor limits the maximum incident laser power ($\sim 50\,\mu\mathrm{W}$) that can be used for OHD cw-CRD detection without saturating the photodetector PD_1. The same laser power limit does not apply to direct, forward-propagating cw-CRD detection, for which the full laser power (~ 5 mW) can be used. Our originally reported [14] noise-limited sensitivity for direct rapidly swept cw-CRD experiments ($7 \times 10^{-8}\,\mathrm{cm}^{-1}$, 8 sweeps averaged, ~ 30 waveforms s^{-1}) was $3.6 \times 10^{-8}\,\mathrm{cm}^{-1}\,\mathrm{Hz}^{-1/2}$. By increasing the laser power as above and with improved data acquisition rate, it has been possible for our direct rapidly swept cw-CRD technique to attain a noise-limited sensitivity of $< 3 \times 10^{-9}\,\mathrm{cm}^{-1}\,\mathrm{Hz}^{-1/2}$, matching that of its OHD counterpart. Moreover, use of a demodulating logarithmic amplifier for more efficient determination of ringdown times τ from the envelope of an OHD cw-CRD waveform (as described in Sect. 3.2 below) does not result in any discernible improvement in noise-limited sensitivity. One possible explanation for this is that the frequency and intensity instabilities of the laser used are predominant, relative to other factors affecting reproducibility of CRD waveforms.

The above form of sensitivity, measured in terms of absorption loss per unit length (e.g. in units of cm^{-1} or $\mathrm{cm}^{-1}\,\mathrm{Hz}^{-1/2}$), is useful as an absolute performance measure. It can be related to a minimum detection limit (MDL) based on concentration or pressure, or to a mixing ratio (e.g. ppm or ppb units). Such MDLs depend on the specific sample conditions and spectral feature examined. For instance, in the case of CO_2 at approximately 1.53 μm, the noise-limited sensitivity obtained in Fig. 5a ($3 \times 10^{-9}\,\mathrm{cm}^{-1}$) for the most intense feature (peak F, $6537.30\,\mathrm{cm}^{-1}$) yields a minimum detectable CO_2 pressure of 37 μbar, provided that the total sample pressure is low enough to maintain Doppler-limited linewidths ($0.012\,\mathrm{cm}^{-1}$ FWHM). For gas samples measured at atmospheric pressure (e.g. by dilution of CO_2 in air), pressure broadening needs to be considered in addition to Doppler broadening. This effectively degrades the minimum pressure at which a dilute species can be detected because peak heights are reduced and overlapping of spectral lines is increased (by a factor of ~ 14 between 50 mbar and 1 bar). Use of peak F at $6537.30\,\mathrm{cm}^{-1}$ for trace detection of CO_2 in "CO_2-free" air at a total pressure of 1 bar therefore yields an estimated MDL of 0.52 mbar (520 ppm).

The result for peak F discussed above applies to the relatively weak R(50) transition of the 1.54-μm $(30^01)_\mathrm{I}$ – (00^00) band of CO_2; the most intense peaks in the same band (e.g. R(14) at $6514.25\,\mathrm{cm}^{-1}$) are approximately 29-times stronger and would therefore enable a minimum neat CO_2 pressure of approximately 1.3 μbar to be detected by the same OHD cw-CRD approach. For a sample of CO_2 diluted in air to a total pressure of 50 mbar (above which pressure broadening becomes dominant over Doppler broadening), this would correspond to a MDL of approximately 26 ppm. The corresponding MDL for CO_2 in air at 1 bar would be approximately 18 ppm, after allowing for pressure broadening. Lower MDLs (~ 2 ppm in air at 1 bar) are projected by tuning to the nearby 1.57-μm $(30^01)_\mathrm{II}$ – (00^00) band which is approximately eight-times more intense [23] than the 1.54-μm $(30^01)_\mathrm{I}$ – (00^00) band to which peak F (Fig. 5) belongs.

Such projected detection limits, for CRD spectroscopy in weak combination bands, are attained with relatively inexpensive 1.55-μm communication-band instrumentation. The fundamental bands of CO_2, namely, (00^01) – (00^00) at approximately 4.2 μm and (01^10) – (00^00) at approximately 15.0 μm [22], have 'rotationless' vibrational band strengths [23] that are respectively 1.6×10^6- and 1.4×10^5-times greater than for the 1.54-μm $(30^01)_\mathrm{I}$ – (00^00) combination band that is of primary interest here (e.g. peak F in Fig. 5). Sub-ppb sensitivity for CO_2 in air is attainable [26] in the 4.2-μm ν_3 fundamental absorption region by Fourier-transform infrared (FTIR) spectroscopy in a high-throughput multipass absorption cell. CRD-based detection of CO_2 in air is likewise expected to have particularly high sensitivity in the 4.2-μm and 15.0-μm fundamental absorption regions, compared to combination bands in the vicinity of 1.55 μm. However, this would require substantial (costly) changes in TDL wavelength, ringdown cavity mirrors, photodetector and other optical elements.

Many other gas-phase molecules can be monitored by means of communication-band TDLs at approximately 1.55 μm, many with higher projected CRD-spectroscopic sensitivities than CO_2. Such gases include acetylene (C_2H_2), ammonia (NH_3), carbon monoxide (CO) and hydrogen cyanide (HCN). MDLs for these and other gases at approximately 1.55 μm can be estimated from data in the HITRAN'96 database [22] and projected on the basis of the noise-limited sensitivity for OHD cw-CRD absorption detection that we have demonstrated above (i.e. $3 \times 10^{-9}\,\mathrm{cm}^{-1}$). Improved detection limits can be achieved (at least in principle!) by using more strongly absorbing spectroscopic features, provided that suitable mid-infrared laser sources and other optical components are available at appropriate wavelengths.

3 Refinements of rapidly swept cw-CRD instrumentation

In this Section, we consider some specific instrumental refinements of our rapidly swept cw-CRD technique that have not previously been reported.

3.1 *Internal calibration of wavelength-scan linearity*

Another OHD cw-CRD scan of a portion of the same spectrum of CO_2 gas as in Fig. 5a is presented with even higher definition in Fig. 6. Above it, a simultaneously recorded wavelength-calibration plot (b) registers deviations from non-linearity of the scan of wavelength of the cw TDL. This wavelength-calibration plot is obtained by recording the voltage that is applied to the PZT by the optical cavity-length controller at the instant at which the leading edge of the build-up and ringdown signal transient waveform triggers the digital oscilloscope in the control electronics. The ringdown cavity thereby serves conveniently and economically as an automatic reference étalon, as well as performing its primary spectroscopic function. This feature enables the resonance point of a remotely located, rapidly swept ringdown cavity to be calibrated simply as the input wavelength of the cw laser is slowly scanned, avoiding extra components usually needed to generate wavelength markers and calibrate wavelength-scan non-linearities.

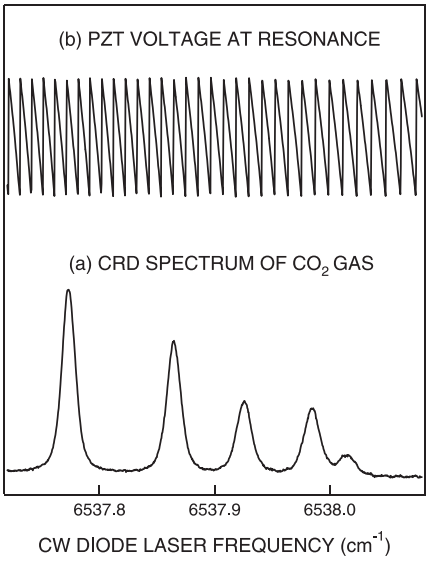

FIGURE 6 Another OHD cw-CRD scan (a) of a portion of the same spectrum of CO_2 gas, as in Fig. 5a. The simultaneously recorded wavelength-calibration plot (b) registers deviations from non-linearity of the scan of wavelength of the cw TDL; this is monitored from resonant PZT voltages applied to the rapidly swept ringdown cavity, which serves automatically as a reference étalon. Note that the abscissa scale is not exactly linear

3.2 *Direct processing of OHD cw-CRD envelopes by demodulating amplifier*

In our previous reports of rapidly swept OHD cw-CRD spectroscopy [9, 15], the ringdown time τ was extracted by performing full-wave rectification of oscillating waveforms, such as Fig. 3, and then the rectified waveform was smoothed with a time constant that was much less than the ringdown time. The full-wave rectification approach loses the advantage that OHD cw-CRD signals decay twice as slowly as direct (non-OHD) signals, as already discussed above in the context of (1).

There is a better way to process OHD cw-CRD signals, as illustrated in Fig. 7, which presents three cw-CRD signal waveforms recorded simultaneously in a single sweep of the ringdown cavity. Figure 7a shows a direct, forward-propagating cw-CRD waveform, similar to that in Fig. 3a. Figure 7b shows an unprocessed OHD cw-CRD waveform, as in Fig. 3b, while Fig. 7c has been generated by passing the unprocessed waveform (b) through a commercially available demodulating logarithmic amplifier (Analog Devices model AD8307, bandwidth DC – 500 MHz, linearity ±1 dB, dynamic range 92 dB). This approach directly converts the exponentially decaying full-wave envelope of the optical heterodyne oscillations, as depicted in Fig. 7b, into a smooth linear decay (c), the slope of which provides a ready means of measuring the ringdown time τ.

This new "demodulating logarithmic amplifier" approach is much more convenient than the "rectify-and-smooth" method that was previously used [9, 15] to generate an exponential decay curve from the full-wave envelope. Moreover, the use of a demodulating logarithmic amplifier, as in Fig. 7c, advantageously preserves the two-fold slower decay rate $(2\tau)^{-1}$ of the full-wave envelope in Figs. 3b and 7b, relative to the previously used [9, 15] rectified decay rate τ^{-1}. In addition, direct measurement of the envelope of the oscillating OHD cw-CRD waveform avoids problems usually encountered in extracting τ from an oscillating waveform and enables a much larger portion of the cavity-sweep time range to be

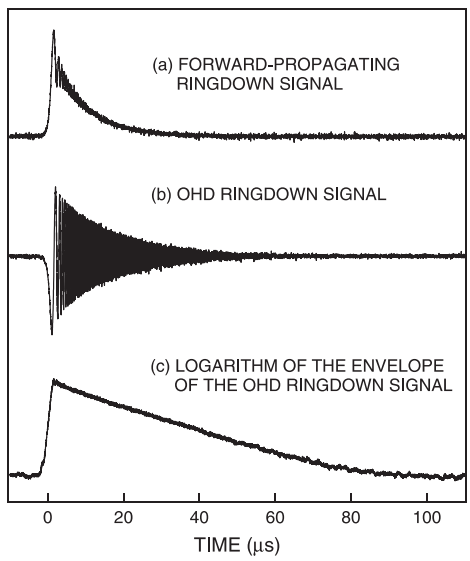

FIGURE 7 Three cw-CRD signal waveforms recorded simultaneously in a single sweep of the ringdown cavity. Figure 7a and b are similar to Fig. 3a and b and Fig. 4a and b, except that the effective mirror reflectivity is now higher ($R = 0.99983$) and the ringdown time, $\tau = 8.62\,\mu s$. Plot (a) shows a direct, forward-propagating cw-CRD waveform; its decay is of form $e^{-t/\tau}$. Plot (b) shows an unprocessed OHD cw-CRD waveform; the decay of its envelope is of form $e^{-t/2\tau}$, twice as slow as in plot (a). Plot (c) is generated by passing the unprocessed waveform (b) through an AD8307 demodulating logarithmic amplifier to directly convert the exponentially decaying full-wave envelope (b) into a smooth linear decay (c) with a slope of $-0.252\,dB\,\mu s^{-1}$

used for this process. Note, too, that the AD8307 demodulating logarithmic amplifier automatically suppresses and damps out wild, noise-derived oscillations that usually arise when the true logarithm of the tail of a decaying signal is recorded.

3.3 *Fibre-optical coupling in a rapidly swept cw-CRD spectrometer*

We have already demonstrated, in the context of Fig. 2 above, that our OHD cw-CRD system naturally yields an advantageous single-ended configuration, with both the optical transmitter and receiver collocated in a single console that can be widely separated from the rapidly swept ringdown cavity module. We can further enhance this advantage by using optical fibre to couple the transmitter-and-receiver console to the ringdown cavity module, replacing simple free-space light propagation (as in Fig. 2). The fibre-optical approach to OHD cw-CRD instrumentation is illustrated in Fig. 8.

This is the first of several embodiments of our OHD cw-CRD technique in which optical fibres are used to transmit the radiation over various portions of the beam path. Standard single-mode optical fibres are typically optimised to operate in individual wavelength ranges (e.g. 1.5 to 1.8 microns), but an optical fibre optimised for one wavelength can still be used with single-mode characteristics at longer wavelengths, but usually with inferior input coupling efficiency and optical transmission characteristics. (A single-mode optical fibre necessarily operates multi-mode at shorter wavelengths below its cut-off wavelength.) Accordingly, it is possible for suitably selected single-mode optical fibres to cover the entire spectral range from the visible to the near infrared.

Figure 8 shows schematically how a single-mode optical fibre can be used to transmit the cw laser beam from the (left-hand) OHD transmitter-and-receiver section to the (right-hand) ringdown cavity module via microscope objective lenses. The ringdown cavity module can therefore be remotely located and connected to the main instrumental control system solely by the optical fibre (which carries the forward-propagating laser light field, $\boldsymbol{E}_{\mathrm{L}}$, and the backward-propagating OHD light fields, $\boldsymbol{E}_{\mathrm{I}}$ and $\boldsymbol{E}_{\mathrm{B}}$, reflected from the ringdown cavity) and an electrical cable carrying the optical cavity-sweep voltage to the PZT element.

It is important to be able to control the polarisation of the backward-propagating light returning to the OHD receiver. A mechanical fibre-polarisation manipulator (not explicitly shown in Fig. 8) is typically needed to adjust the polarisation of the light that the fibre transmits in both directions. We prefer to use single-mode optical fibre rigidly mounted in a conduit (so that it cannot be twisted or experience polarisation-shifting vibrations) rather than use polarisation-preserving fibre (which usually generates an ellipse-shaped beam profile). This problem of the polarisation of the backward-propagating light can be greatly diminished by replacing the "polarisation control" section of the apparatus (Figs. 2 and 8) by an optical three-port circulator, a bulk micro-optical device that is in common use in the photonics/telecommunications industry. Optical circulators are insensitive to variations in the polarisation of the light that they transmit; their proposed use in an all-fibre-optical OHD cw-CRD spectroscopic system will be discussed in Sect. 5, below. Another variation of the single-ended, fibre-coupled apparatus depicted in Fig. 8 could locate the PZT voltage supply close to the ringdown cavity and transmit control signals to and from the OHD transmitter-and-receiver console by another optical fibre or by wireless means. Any of these approaches yields a single-ended OHD cw-CRD optical detection system with the relatively inexpensive, rugged ringdown cavity section widely separated from the transmitter-and-receiver instrumental control system.

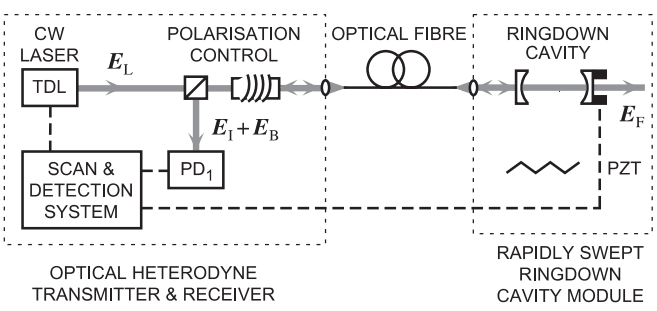

FIGURE 8 Schematic of a fibre-coupled, swept-cavity OHD cw-CRD spectrometer. This is similar to Fig. 2, except that optical fibre is used to carry light between the transmitter-and-receiver console and the rapidly swept ringdown cavity module. Notation is as in Fig. 2

Experimental cw-CRD results, such as those presented in Figs. 6 and 7, have been successfully recorded with light transmitted in this way to and from the ringdown cavity by a 12-m length of single-mode optical fibre. It is remarkable that, by careful optical alignment, we are able to achieve efficient coupling into the single-mode optical fibre of both the incident laser light and the counter-propagating light reflected from the rapidly swept ringdown cavity.

A further extension of the single-ended, fibre-coupled approach to a rapidly swept OHD cw-CRD spectroscopic system (as depicted in Fig. 8) entails using numerous ringdown cavities, each coupled by a single-mode optical fibre and a PZT control link to a single central transmitter-and-receiver console. A suitable fibre-optical splitter or switch module can be used to distribute the incident laser light and the return ringdown light to and from different locations of a site at which the various ringdown cavities are positioned. This approach enables the "input" and "output" components of the overall apparatus to be in a central, accessible, secure location (where the instrument operator is) such as an air-conditioned control room, communicating with miniature rugged ringdown cavities that are distributed in more hostile and/or less accessible locations (where the molecules are). For instance, a fibre-coupled network of ringdown cavities could be distributed at various gas effluent sources on an industrial, environmental or agricultural site, or used for diagnostic breath analysis in a series of hospital wards. Prospects for such measurements will be discussed in Sect. 5 below.

4 Spectroscopically tailored, multi-wavelength detection

One of the distinctive advantages of our rapidly swept OHD cw-CRD spectroscopic method is that it is readily amenable to multi-wavelength, multi-species detection. Such an approach is an example of what we call "spectroscopic tailoring", in which light from a coherent spectroscopic light source is discretely structured to match characteristic features

of the target of interest (as well as reference non-resonant wavelengths), thus offering a substantial multiplex advantage for spectroscopic sensing applications.

Figures 9 and 10 illustrate two single-ended, multiplex variants of a rapidly swept OHD cw-CRD spectrometer, similar in some respects to those in Figs. 2 and 8. The new feature is that the single TDL (the wavelength of which is usually slowly scanned) in Figs. 2 and 8 is now replaced in Figs. 9 and 10 by a set of fixed-wavelength diode lasers (DL_1, DL_2, DL_3, ...) with their output beams combined spatially, directionally and with preserved linear polarisation. This is achieved by coupling each laser beam (by means of beam-steering reflectors and/or beam splitters and a microscope objective lens) into a short length ($\sim$ 1 m) of single-mode optical fibre. The light emerging from the other end of the optical fibre is collected by a second microscope objective lens such that all the laser beams (from DL_1, DL_2, DL_3, ...) are co-aligned, propagating with common spatial characteristics. This is necessary to ensure that all laser beams are efficiently coupled simultaneously into the one ringdown cavity. The remaining optical paths in Figs. 9 and 10 are as in Figs. 2 and 8, respectively, with fibre-optical coupling to the ringdown cavity in the cases of Figs. 8 and 10.

As mentioned above, each cw laser DL_1, DL_2, DL_3, ... is set to emit at a particular characteristic wavelength. Some of these wavelengths are chosen to be resonant with spectroscopic features of gas-phase chemical species that are of particular interest. At least one other wavelength is chosen such

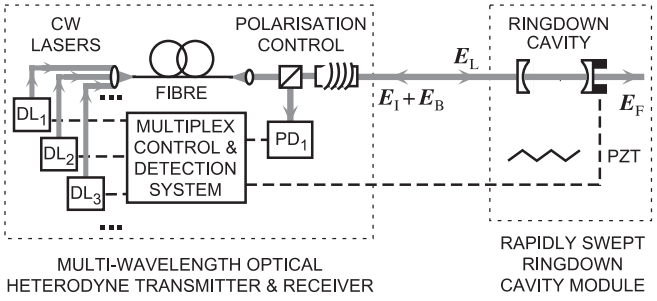

FIGURE 9 Schematic of the multi-wavelength version of a swept-cavity OHD cw-CRD spectrometer. This is similar to Fig. 2, except that the single, slowly scanned TDL is replaced by a group of fixed-wavelength diode lasers (DL_1, DL_2, DL_3, ...) with their output beams combined via a short length of single-mode optical fibre to co-propagate into the one ringdown cavity. Notation is as in Figs. 2 and 8

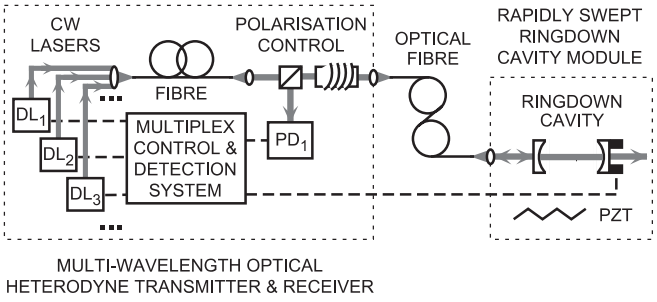

FIGURE 10 Schematic of the multi-wavelength version of a fibre-coupled, swept-cavity OHD cw-CRD spectrometer. This is similar to Fig. 9, except that optical fibre is used to carry light between the transmitter-and-receiver console and the rapidly swept ringdown cavity module. Notation is as in Figs. 2, 8 and 9

that it is removed from any known spectroscopic features, in order to measure the non-resonant background or baseline. Such background reference points need to be carefully checked using "zero" gases (e.g. CO_2-free synthetic air) in the sample cell. The ringdown cavity is rapidly swept as previously described in Sects. 2 and 3 above. Chemical species that are typically of interest usually have many characteristic optical absorption features within a narrow wavelength range. This provides flexibility in the setting of laser wavelengths. We note that such a "point-sampling" approach to spectroscopic sensing needs very careful setting-up and calibration if it is to be at all competitive with the more straightforward approach of scanning a full spectrum. The relatively high rate at which analytically significant data can be acquired in the former (point-sampling) approach is traded off against the full lineshape and baseline information that is available in the latter (spectrum scan) approach.

The length of the ringdown cavity at rest is an important additional adjustable parameter. Laser wavelengths and the optical cavity length are precisely set to ensure that the cw-CRD waveforms for each of the different wavelengths from the cw lasers DL_1, DL_2, DL_3, ... occur at a different point in the optical cavity-sweep cycle. Each of these build-up and ringdown transient waveforms must be clearly separated (e.g. by a few cavity ringdown time intervals) from any other ringdown waveform to avoid unwanted interference effects. It is then possible, after careful adjustment of the ringdown cavity length (and hence its free spectral range) to collect cw-CRD spectroscopic signals for several (e.g. 2–5 channels) characteristic spectroscopic features for different absorbing species and non-resonant background reference points.

All of these spectroscopically tailored cw-CRD detection channels can be detected effectively simultaneously, within a single rapid sweep period (typically less than 1 ms) of the ringdown cavity. We note an earlier multiplex cw-CRD spectroscopic study [27], in which AO switches toggled between two 1.4-μm TDLs tuned to absorption features of vapour-phase species such as methanol and isopropanol.

A two-channel demonstration of this principle is shown in Figs. 11 and 12, with two separate optical-fibre-coupled TDLs (each New Focus model 6262/6200) in an apparatus configured as in Fig. 10 and with a 12-m length of optical fibre used to couple the OHD transmitter-and-receiver section of the apparatus to the rapidly swept ringdown cavity module. One of the two TDL wavelengths (yielding cw-CRD waveforms on the right-hand side of the plot) is typically set to coincide with a characteristic optical absorption wavelength of the gas of interest. The other TDL wavelength is set at an off-resonance wavelength to yield OHD cw-CRD waveforms (on the left-hand side of the plots in Figs. 11 and 12) that are effectively those of the empty ringdown optical cavity. Figure 11 shows two pairs of OHD cw-CRD waveforms: (a) full oscillating waveform, and (b) demodulating logarithmic amplifier output. Each plot was recorded in the same single sweep of the cavity, with the two cw TDL output intensities pre-set to yield cw-CRD signals of approximately equal amplitude. These were recorded when the optical cavity was empty (i.e. before CO_2 gas was admitted to the cell).

Corresponding cw-CRD results, obtained with CO_2 gas at a pressure of 2 mbar in the cell, are shown in Fig. 12. Minor

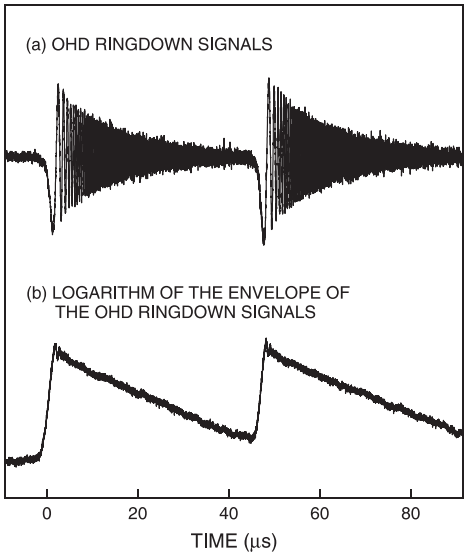

FIGURE 11 Rapidly swept signals from a dual-wavelength OHD cw-CRD spectrometer. Plot (a) shows a pair of raw OHD cw-CRD waveforms, each as in Fig. 3b but collected quasi-simultaneously at separate points in the cavity-sweep cycle. Plot (b) is generated by passing the raw waveforms (a) through an AD8307 demodulating logarithmic amplifier. Each plot was recorded in the same single sweep of an empty ringdown cavity, with the two cw TDL output intensities pre-set to yield approximately equal amplitudes

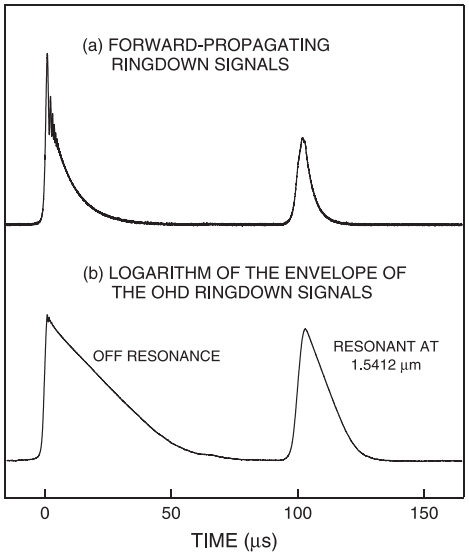

FIGURE 12 Rapidly swept signals from a dual-wavelength cw-CRD spectrometer, recorded with CO_2 gas at a pressure of 2 mbar in the ringdown cavity cell. The cavity length is adjusted so that each laser wavelength becomes resonant with the cavity at a distinct point in the sweep cycle, thereby allowing quasi-simultaneous detection of signals that are respectively on-resonance (*right-hand waveforms*) and off-resonance (*left-hand waveforms*) with the absorbing molecules of interest (CO_2 gas in this case). These results differ from those in Fig. 11 as follows: plot (a) is now recorded in direct, forward-propagating (non-OHD) mode; 256-sweep averages are taken concurrently; the *right-hand waveforms* correspond to an on-resonance TDL wavelength coinciding with the 1.5412-μm P(18) absorption line of CO_2 gas. Optical absorption by CO_2 molecules causes a decrease of both cw-CRD signal amplitude and ringdown time for the right-hand on-resonance waveforms relative to the left-hand off-resonance waveforms

adjustments have been made to set the "on-resonance" TDL wavelength to 1.5412 μm (6488.355 cm^{-1}), coinciding with the prominent P(18) peak in the 6503-cm^{-1} $(30^01)_I - (00^00)$ rovibrational optical absorption band of CO_2 gas [22]. These adjustments have caused the sweep-time separation between the two cw-CRD waveforms to be increased from approximately 45 μs in Fig. 11 to approximately 100 μs in Fig. 12. Each of the two traces (a, b) depicted is a 256-shot average, respectively recorded (a) by detecting the forward-propagating cw-CRD signal, as in Fig. 3a and (b) by using the demodulating logarithmic amplifier to register OHD cw-CRD signals, as in Figs. 7c and 11b. The effect of optical absorption by CO_2 molecules is evident as a decrease of both cw-CRD signal amplitude and ringdown time for the right-hand waveforms (i.e. those coinciding with the 1.5412-μm P(18) absorption line of CO_2 gas). The leading edges of the left-hand cw-CRD waveforms (i.e. those for an off-resonance wavelength) are used to trigger the digital oscilloscope. These auto-triggered (left-hand) waveforms are more sharply defined than the subsequent (right-hand) waveforms, owing to a short-term optical frequency instability of approximately ±1 MHz for each TDL employed and the fact that these results were obtained as a 256-sweep average. It should be noted that this is a crude demonstration of dual-wavelength cw-CRD spectroscopy, in that the reserve cw-CRD spectroscopic detection sensitivity spans many orders of magnitude. It is therefore capable of measuring much smaller concentrations of CO_2 gas than in this proof-of-principle example.

It is necessary to ensure that the wavelengths of the various cw lasers DL_1, DL_2, DL_3, ... in Figs. 9 and 10 are separated by optical frequency intervals that exceed the response frequency or bandwidth of the photodetector (PD_1). This precaution is needed to avoid complications from unwanted difference frequencies. For a typical photodetector, this bandwidth limit is typically less than a few GHz.

Another necessary adjustment in these multi-wavelength cw-CRD configurations is to vary the linear polarisation of each of the cw laser beams so that light emerging from the beam-combining optical fibre has a common polarisation orientation. We used a simple mechanical optical-fibre polarisation manipulator to adjust the polarisation orientation of the light emerging out of the single-mode optical fibre, so that its linear polarisation axis matched that of the polarisation control unit shown in Figs. 9 and 10. The need for such polarisation-control measures can be minimised by using a polarisation-insensitive fibre-optical circulator in place of the "polarisation control" section of Figs. 9 and 10 (as already mentioned in Sect. 3.3 above and further discussed in Sect. 5 below).

In implementing multi-wavelength, fibre-coupled, rapidly swept cw-CRD spectroscopy (such as the scheme depicted in Fig. 10), it is feasible to use standard telecommunication optical fibre that is optimised for the shortest wavelength (highest optical frequency) of the set of cw lasers DL_1, DL_2, DL_3, ... used. The other longer wavelengths (lower optical frequencies) of the remainder of the set is then above the cut-off wavelength of the optical fibre, so that the fibre remains single-mode for radiation from the entire set of cw lasers. For example, an optical fibre designed for single-mode operation in the telecommunications C band (in the near-infrared wavelength range 1.53–1.57 μm) can serve as a single-mode fibre at longer wavelengths with acceptable transmission characteristics extending to longer infrared wavelengths (e.g. 2.5 μm and beyond).

The wavelength-dependence of other components in the multi-wavelength rapidly swept cw-CRD spectrometer (such as those depicted in Figs. 9 and 10) also needs to be considered. The ringdown cavity mirrors can be made with high-reflectivity dielectric coatings optimised for a particular wavelength but still yielding acceptably high reflectivity over a useful range of wavelengths (e.g. 1.5–2.5 μm) of the set of cw lasers DL_1, DL_2, DL_3, used. Such wavelength dependence of mirror reflectivity causes the empty-cell ringdown time to vary for each of the cw lasers, with longest ringdown times for the wavelength(s) at which the mirror reflectivity is optimised; such variations are readily taken into account in the CRD-spectroscopic analysis procedure. The polarisation control optics section of the multi-wavelength optical heterodyne cw-CRDS apparatus, as in Figs. 9 and 10, typically comprises a polarising beam splitter and either a Faraday rotator or a quarter-wave optical retarder. Prism polarisers are available for use over a wide range of wavelengths, although other types (e.g. thin-film plate polarisers) are efficient over a more limited wavelength range. The rotation angle of a Faraday rotator and the quarter-wave thickness of an optical retarder plate are each dependent on the wavelength (or optical frequency) of the light and therefore are designed with a centre wavelength appropriate for one of the laser wavelengths used and acceptable characteristics at other wavelengths in the set. The polarisation control optics unit will therefore have a reduced coupling efficiency for backward-propagating light at wavelengths far removed from the unit's designed centre wavelength, limiting the optical power reaching the photodetector (PD_1) and reducing the signal-to-noise ratio accordingly. The transmission characteristics of optical materials (such as fused silica) also limit the range of wavelengths that are applicable, but this is not a severe restriction in the near-infrared and visible regions, where our initial implementations of the technique are concentrated. For instance, standard silica-core optical fibre typically has an attenuation characteristic of 0.3 dB per kilometre over the wavelength ranges of 0.90–1.42 μm and 1.46–1.90 μm; special silica-core optical fibres with low OH (hydroxyl) optical absorption are available to minimise transmission losses in the 1.42–1.46 μm region. The wavelength range of 1.9–3.0 μm is accessible by using infrared fluoride-glass fibres. Other developments in fibre-optical materials promise to extend the accessible wavelength range for future applications.

Our multiplex, spectroscopically tailored cw-CRD technique is intrinsically and uniquely reliant on a rapidly swept ringdown cavity and a single-ended OHD transmitter-and-receiver configuration. It is able to make multi-species concentration measurements that are effectively simultaneous on the timescale of many gas-phase processes of interest. In many applications (e.g. with a static sample in the optical cavity), the timescale of fluctuations of the absorbing medium is long relative to the cavity sweep period and successive multiplex cw-CRD can be accommodated within that period. It is then possible to average over successive cavity sweeps to enhance the signal-to-noise ratio and CRD spectroscopic sensitivity. In other applications, for example with a turbulent or rapidly reacting sample in the optical cavity, signal averaging is no longer feasible to enhance sensitivity and there may be significant fluctuations between single-shot multiplex build-up and decay transient waveforms in successive optical-cavity sweep cycles.

5 Concluding remarks

5.1 *Photonics technology meets cavity ringdown*

In this paper, we demonstrate much of the potential of rapidly swept cw-CRD spectroscopic techniques for trace gas detection. Our single-ended OHD approach is especially promising, in that it offers enhanced sensitivity and enables the main transmitter-and-receiver console to be widely separated from one or more ringdown cavity modules distributed in locations where gases need to be monitored. The use of fibre-optical coupling provides additional flexibility and convenience. Optical fibres are also a key to multi-wavelength variants of cw-CRD spectroscopy, in that they enable the output beams from a group of lasers, each preset to a characteristic on- or off-resonance wavelength, to be merged to co-propagate in a single ringdown cavity. The cavity length is adjusted so that each laser wavelength is resonant at a distinct point in the sweep cycle, thereby allowing quasi-simultaneous detection of several gas-phase species and related non-resonant background reference signals.

The potential of this approach can be extended by taking advantage of the full scope of modern photonics and optical telecommunications technology. An example is presented schematically in Fig. 13. This proposed single-ended, multiplex, fibre-coupled OHD cw-CRD spectrometer is an integrated system incorporating standard photonics components such as: compact, single-longitudinal-mode DFB-type TDLs (with their output wavelengths controlled by current and temperature); pigtail-couplers on lasers, detectors and optical fibres (replacing discrete microscope objective lenses and fibre-optic micropositioners); optical isolators (integrated into the optical fibres to protect each diode laser from unwanted optical feedback); a wavelength division multiplexer (combining the various cw laser beams into a single-mode optical fibre, by means of a $N \times 1$ combiner/multiplexer); a three-port optical circulator (a micro-optical device that replaces the function of discrete polarisation-control optics). It has already been noted in Sects. 3 and 4 that optical circulators are insensitive to variations in the polarisation of the light, which is advan-

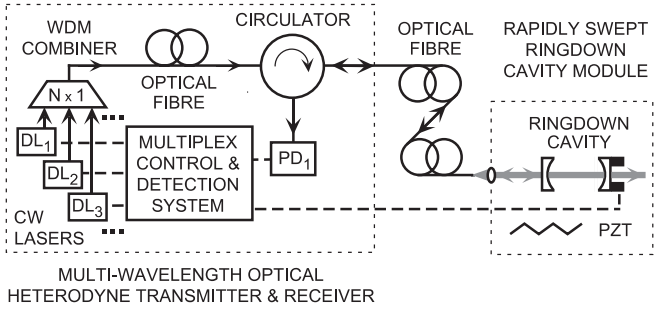

FIGURE 13 Schematic of a proposed single-ended, multiplex, fibre-coupled OHD cw-CRD spectrometer, packaged as an integrated system incorporating standard photonics components. This is similar in some respects to Fig. 10, except that fibre-pigtailed optical components are used throughout (apart from the ringdown cavity itself, which is intrinsically a free-space optical device). Also, a polarisation-insensitive optical circulator here replaces the discrete polarisation-control optics previously used in Figs. 2 and 8–10

tageous in this application. Photonics devices such as those depicted in Fig. 13 are widely used in fibre-optical telecommunications instruments. The OHD transmitter-and-receiver system and the ringdown cavity module are thereby packaged with fibre-optical pigtail connectors so that different parts of the system are linked entirely through optical cables (apart from the ringdown cavity itself, which is intrinsically a free-space optical device requiring a discrete coupling lens and fibre-optic micropositioner).

We are currently constructing a portable prototype of the rapidly swept OHD cw-CRD spectrometer based on communications-band photonics components as depicted in Fig. 13. This prototype is designed to provide a convenient, rugged, economical means of trace gas detection to be used in the field for industrial, medical, agricultural or environmental sensing.

5.2 *Near-infrared communication-band gas-sensing applications*

Accurate, real-time measurement of gas concentrations is important in medical, industrial, agricultural and environmental diagnostics. As explained above, our various forms of rapidly swept cw-CRD spectroscopy show promise as an economically cheap, compact, rugged and non-invasive means of laser-based gas analysis. There is no shortage of significant gas-sensing applications, even with a rapidly swept cw-CRD spectrometer confined, by readily available photonics technology, to the regular near-infrared communications band (1.52–1.62 μm). Key gas-phase molecular species that are amenable to sensing by rapidly swept cw-CRD spectroscopy in this wavelength region [22] define the market potential of our technique. Some target applications are outlined below.

Applications of our rapidly swept cw-CRD spectroscopic techniques to sensing of CO_2 gas have been discussed in detail in Sects. 2 and 3 above. Rovibrational absorption bands of CO_2 that are of particular relevance in the wavelength range of 1.52–1.67 μm are $(30^01)_{\mathrm{I}} - (00^00)$ and $(30^01)_{\mathrm{II}} - (00^00)$, as well as the Q-branch of $(11^12)_{\mathrm{II}} - (00^00)$ that is prominent in Fig. 5. It is known [28] that the second of these three bands is overlapped in the vicinity of 1.56–1.59 μm by the second overtone (3–0) band of carbon monoxide (CO). This spectroscopic coincidence offers the prospect of simultaneous detection of CO_2 and CO gases, as has already been recognised in previous TDL absorption studies [29].

The gas-phase ratio of CO to CO_2 is known to be a key control measure of combustion efficiency in industrial processes such as smelting, where incomplete combustion or inefficient conversion of hydrocarbon fuels results in a higher relative concentration of CO. Spectroscopic, laser-based detection of the CO/CO_2 ratio in combustion effluent streams (e.g. industrial smokestacks) offers the prospect of real-time combustion process control and/or environmental monitoring of air quality. Laser-based sensing has been applied to this problem in a basic oxygen steel furnace, using relatively exotic, fragile, cryogenically cooled mid-infrared lead-salt TDLs at 4.5–5.5 μm. Here, the fundamental (1–0) rovibrational absorption band of CO overlaps the $(00^01)_{\mathrm{I}} - (00^00)$, $(11^10)_{\mathrm{I}} - (00^00)$ and $(11^10)_{\mathrm{II}} - (00^00)$ bands of CO_2. Line-of-sight measurements of temperature and CO/CO_2 concentration ratios have been made on steel furnace off-gases during oxygen blowing [30]. The multi-wavelength/species version of our OHD cw-CRD technique promises to yield competitive detection sensitivities and data collection rates, together with simpler instrumentation for such measurements. As explained in Sect. 4, a major advantage of our multiplex rapidly swept cw-CRDS method is that each of the species of interest is monitored virtually simultaneously (within ~ 1 ms at most), rather than having to scan actively from one characteristic wavelength to another. We note again a previous non-OHD multiplex cw-CRDS study [27] in which AO modulators alternate between two characteristic 1.4-μm diode laser wavelengths.

Likewise, there are numerous medical applications that rely on breath analysis of gases that a patient exhales [31]. Some of these involve detection of CO and/or CO_2 gases. For example, human breath analysis of CO (absorbing at 1.56–1.59 μm) and CO_2 (absorbing at 1.52–1.67 μm) can be used to diagnose neonatal jaundice or asthma. The presence of CO in a patient's breath also reveals blood condition, hæme protein metabolism, cardiovascular disease and nerve transmission, while CO_2 in human breath indicates gastric, liver, intestinal, pancreatic and bowel disease, and blood/lung gas interchange (in ratio to O_2). Isotopically labelled $^{13}CO_2$ is monitored in non-invasive diagnosis of gastritis and peptic ulcers arising from bacterial infection by Helicobacter pylori, as addressed in a recent report of high-sensitivity cw-CRD spectroscopy [24].

There are important applications involving the sensing of hydrocarbon gases. Dependable detection of acetylene (C_2H_2, absorbing at 1.52–1.54 μm) in the presence of other hydrocarbons (alkenes and alkanes) is needed to control catalytic cracking efficiency in the petroleum industry. Likewise, breath analysis of light alkane gases (C_nH_{2n+2}, $n = 1$–3, absorbing at 1.4–1.7 μm) can be used to diagnose various medical conditions: heart, lung, colon and bowel disease; stroke; arthritis; schizophrenia; multiple sclerosis; vitamin E and trace element deficiency. Methane (CH_4, absorbing at 1.63–1.70 μm [32]) is a key indicator gas in agriculture, industry and the environment of issues such as dairy cattle health, natural gas supply safety, atmospheric chemistry and combustion diagnostics.

Another potential application for rapidly swept cw-CRD spectroscopy includes detection of ammonia gas (NH_3, absorbing at 1.50–1.68 μm [33]). This is a product of protein degradation and so can be used to monitor kidney and liver disease by human breath analysis. Likewise, gas-phase sensing of NH_3 has important applications in agriculture (e.g. fertiliser dispersal), industry (e.g. leak detection, combustion diagnostics) and the environment (e.g. nitrogen cycle, air quality).

5.3 *What next for rapidly swept cavity-ringdown spectroscopy?*

At the outset of this article, we noted that CRD spectroscopy is now a mature, well established technique [1–4]. This raises the question whether any significant advantages for trace gas detection and environmental sensing can be gained by adopting new rapidly swept cw-CRD approaches that we have previously developed [9, 14, 15] and

further described above. It should be evident, from the results presented and the instrumental extensions proposed, that we consider our techniques to have several distinctive features, as follows:

- *Simple, economical design*, with a minimal number of components (mostly standard) and not needing expensive AO or EO switches.
- *Single-ended configuration*, with the swept-cavity OHD approach enabling a central transmitter-and-receiver unit with one or more remotely located ringdown cavity modules.
- *Wavelength-scan linearity*, monitored internally from resonant PZT voltages applied to the rapidly swept ringdown cavity itself.
- *High sensitivity and photometric precision*, enhanced by using a demodulating amplifier to extract ringdown times directly from the envelope of oscillating OHD CRD waveforms.
- *Fibre-optical coupling*, enabled by the swept-cavity OHD approach.
- *Multi-wavelength, multi-species detection*, with several characteristic cw-CRD waveforms collected quasi-simultaneously at separate points in the cavity-sweep cycle.
- *Advanced compact, rugged photonics system*, under development as depicted in Fig. 13.

The noise-limited sensitivity of our rapidly swept OHD cw-CRD spectroscopic technique has been demonstrated in the context of Sect. 2.4 to be $2.5 \times 10^{-9}\,\mathrm{cm}^{-1}\,\mathrm{Hz}^{-1/2}$. While this is competitive with many established forms of CRD spectroscopy [1–4], it falls short of recently reported state-of-the-art CRD measurements [24]. We repeat that our current objective is to concentrate on relatively simple, compact, economical cw-CRD spectrometer designs, rather than to seek the highest possible detection sensitivity. The resulting trade-off between sensitivity and instrumental complexity is self-evident.

To attain much higher sensitivity, it would be necessary for us to use higher-reflectivity mirrors, more stable lasers, better ringdown cavity design (e.g. longer pathlength, higher mechanical stability and sweep linearity) and more elaborate high-resolution electronics and feedback circuitry. It should be recognised that such measures would result in greater expense, more complicated instrumentation, a less compact package and a slower data-collection rate. For instance, a 10-fold enhancement of cavity mirror reflectivity (e.g. from $R = 0.9996$ to $R = 0.99996$) might be expected to improve the noise-limited sensitivity (in units of $\mathrm{cm}^{-1}\,\mathrm{Hz}^{-1/2}$) by a factor of $\sqrt{10}$; we note that there would be a 10-fold increase in empty-cavity ringdown time τ, with a corresponding increase in the dwell time to average a given number of sweeps (e.g. 256) and in the wavelength-scan time to record a given span of CRD absorption spectrum.

Practical application of our rapidly swept cw-CRD spectroscopic techniques has so far been confined to the regular near-infrared communications band (1.52–1.62 μm), where suitable lasers, fibre-optical components and other photonic devices are readily available, often at moderate cost. The main disadvantage of this near-infrared region is that the corresponding molecular absorption bands are high-order vibrational overtone and combination bands that are much weaker than lower-order bands (including fundamentals) lying in the mid-infrared region (at wavelengths above 3 μm, say). By extending the infrared wavelength range, it would be possible to attain improved analytical sensitivity (e.g. MDLs in absolute concentration or ppm, ppb, ... units) and to detect many other molecular species. However, this would sacrifice much of the current simplicity of our method, requiring much more exotic components than those available in the communications band at approximately 1.55 μm. Mid-infrared cw coherent light sources that might find future application in rapidly swept cw-CRD spectroscopy include: all-solid-state OPO devices [34, 35]; quantum cascade lasers [36, 37]; difference-frequency generators (e.g. in lithium niobate channel waveguides [38], quasi-phase-matched PPLN [39], or orientation-patterned GaAs [40]); and VCSEL-type TDLs [41]. Two recent reviews address prospects for mid-infrared pulsed and cw OPOs [42].

We have concentrated in this article on continuous-wave cavity ringdown (cw-CRD) spectroscopy, effectively ignoring other promising high-sensitivity variants [1–4], such as cavity-enhanced absorption spectroscopy (CEAS) [14, 43] and integrated cavity output spectroscopy (ICOS) [44] that record the peak height or area of the characteristic build-up and decay waveform, rather than its decay rate. We note in particular that our original rapidly swept cw-CRD spectroscopic measurements [14] included CEAS as a convenient way to extend the dynamic range, and that further rapidly swept cw-CEAS developments have been reported recently [43]. In future work, there may be value in combining the advantageous features of our swept-cavity OHD approach with those of ICOS [44].

This article has been designed to outline trends in our rapidly swept cw-CRD spectroscopic technique and to emphasise its potential for applications to trace gas detection, within the context of this special issue of Applied Physics B – Lasers and Optics. Our concluding message is that various useful forms of laser spectroscopy are available for diagnostic sensing of gases, with our approach deserving a prominent place among them.

ACKNOWLEDGEMENTS We acknowledge financial support from the Australian Research Council and Macquarie University. N. Naidoo assisted us in surveying the literature on the subject of medical gas-sensing applications [31].

REFERENCES

1 J.J. Scherer, J.B. Paul, A. O'Keefe, R.J. Saykally: Chem. Rev. **97**, 25 (1997); J.B. Paul, R.J. Saykally: Analyt. Chem. **69**, 287A (1997)
2 M.D. Wheeler, S.M. Newman, A.J. Orr-Ewing, M.N.R. Ashfold: J. Chem. Soc., Faraday Trans. **94**, 337 (1998)
3 K.W. Busch, M.A. Busch (Eds.): *Cavity-Ringdown Spectroscopy – An Ultratrace-Absorption Measurement Technique, ACS Symposium Series No. 720* (Oxford University Press, Oxford 1999)
4 G. Berden, R. Peeters, G. Meijer: Int. Rev. Phys. Chem. **19**, 565 (2000)
5 A. O'Keefe, D.A.G. Deacon: Rev. Sci. Instrum. **59**, 2544 (1988)
6 D. Romanini, A.A. Kachanov, N. Sadeghi, F. Stoeckel: Chem. Phys. Lett. **264**, 316 (1997)
7 Y. He, M. Hippler, M. Quack: Chem. Phys. Lett. **289**, 527 (1998)
8 G.W. Baxter, M.A. Payne, B.D.W. Austin, C.A. Halloway, J.G. Haub, Y. He, A.P. Milce, J.W. Nibler, B.J. Orr: Appl. Phys. B **71**, 651 (2000)
9 Y. He, B.J. Orr: J. Chinese Chem. Soc. **48**, 591 (2001)

10 Y. He, B.J. Orr: Appl. Opt. **40**, 4836 (2001)
11 M.D. Levenson, B.A. Paldus, T.G. Spence, C.C. Harb, J.S. Harris, R.N. Zare: Chem. Phys. Lett. **290**, 335 (1998)
12 M.D. Levenson, B.A. Paldus, T.G. Spence, C.C. Harb, R.N. Zare, M.J. Lawrence: Opt. Lett. **25**, 920 (2000)
13 J. Ye, J.L. Hall: Phys. Rev. A **61**, 802 (2000)
14 Y. He, B.J. Orr: Chem. Phys. Lett. **319**, 131 (2000)
15 Y. He, B.J. Orr: Chem. Phys. Lett. **335**, 215 (2001)
16 J.W. Hahn, Y.S. Yoo, J.Y. Lee, J.W. Kim, H.W. Lee: Appl. Opt. **38**, 1859 (1999)
17 Z. Li, R.G.T. Bennett, G.E. Stedman: Opt. Commun. **86**, 51 (1991); Z. Li, G.E. Stedman, H.R. Bilger: Opt. Commun. **100**, 240 (1993)
18 K. An, C. Yang, R.R. Dasari, M.S. Feld: Opt. Lett. **20**, 1068 (1995)
19 J. Poirson, F. Bretenaker, M. Vallet, A. Le Floch: J. Opt. Soc. Am. B **14**, 2811 (1997)
20 M.J. Lawrence, B. Wilke, M.E. Husman, E.K. Gustafson, R.L. Byer: J. Opt. Soc. Am. B **16**, 523 (1999)
21 J. Ye, L.S. Ma, J.L. Hall: in [3], Chapt. 15, pp. 233–253; in particular, note Fig. 3, p. 241
22 L.S. Rothman, C.P. Rinsland, A. Goldman, S.T. Massie, D.P. Edwards, J.M. Flaud, A. Perrin, C. Camy-Peyret, V. Dana, J.Y. Mandin, J. Schroeder, A. McCann, R.R. Gamache, R.B. Watson, K. Yoshino, K.V. Chance, K.W. Jucks, L.R. Brown, V. Nemtchinov, P. Varanasi: J. Quantum Spectrosc. Radiat. Transfer **60**, 665 (1998)
23 L.S. Rothman, R.L. Hawkins, R.B. Wattson, R.R. Gamache: J. Quantum Spectrosc. Radiat. Transfer **48**, 537 (1992)
24 E.R. Crosson, K.N. Ricci, B.A. Richman, F.C. Chilese, T.G. Owano, R.A. Provencal, M.W. Todd, J. Glasser, A.A. Kachanov, B.A. Paldus, T.G. Spence, R.N. Zare: Analyt. Chem. **74**, 2003 (2002)
25 J. Ye, L.S. Ma, J.L. Hall: J. Opt. Soc. Am. B **15**, 6 (1998)
26 P.L. Hanst, S.T. Hanst: *Air Monitoring by Spectroscopic Techniques*, ed. by M.W. Sigrist (Wiley-Interscience, New York 1994) pp. 335–470
27 G. Totschnig, D.S. Baer, J. Wang, F. Winter, H. Hofbauer, R.K. Hanson: Appl. Opt. **39**, 2009 (2000)
28 L.I. Gurinovich, V.P. Durayev, V.A. Ivanov, N.K. Nikeyenko: J. Appl. Spectrosc. **62**, 67 (1995)
29 D.M. Sonnenfroh, M.G. Allen: Appl. Opt. **36**, 3298 (1997); R.M. Mihalcea, D.S. Baer, R.K. Hanson: Appl. Opt. **36**, 8745 (1997); B.L. Upschulte, D.M. Sonnenfroh, M.G. Allen: Appl. Opt. **38**, 1506 (1999); J. Wang, M. Maiorov, D.S. Baer, D.Z. Garbuzov, J.C. Connolly, R.K. Hanson: Appl. Opt. **39**, 5579 (2000)
30 D. Otteson, S. Allendorf, P. Ludowise, D. Hardesty, D. Goldstein, T. Miller, C. Smith, M. Bonin: Proc. 81st Steelmaking Conf. **81**, 369 (1998); D. Otteson, S. Allendorf, P. Ludowise, D. Hardesty, D. Goldstein, C. Smith, M. Bonin: Scand. J. Metall. **28**, 131 (1999)
31 M. Phillips: Scientific American, 52 (July 1992); K.D. Thrall, J.J. Toth, S.W. Sharpe: Proc. SPIE – Int. Soc. Opt. Eng. **2676**, 136 (1996); A.I. Kouznetsov, E.V. Stepanov: ibid., 272 (1996); T.A. Dickinson, J. White, J.S. Kauer, D.R. Watt: TIBTECH **16**, 250 (1998); P. Paredi, M.J. Leckie, I. Horvath, L. Allegra, S.A. Kharitonov: Eur. Respir. J. **13**, 48 (1999); L.G. Sandström, S.H. Lundqvist, A.B. Petterson, M.S. Shumate: IEEE. J. Sel. Top. Quantum Electron. **5**, 1040 (1999)
32 V. Nagali, S.I. Chou, D.S. Baer, R.K. Hanson, J. Segall: Appl. Opt. **35**, 4026 (1996)
33 M.E. Webber, D.S. Baer, R.K. Hanson: Appl. Opt. **40**, 2031 (2001)
34 M.E. Klein, C.K. Laue, D.H. Lee, K.J. Boller, R. Wallenstein: Opt. Lett. **25**, 490 (2000)
35 E.V. Kovalchuk, D. Dekorsy, A.I. Lvovsky, C. Braxmaier, J. Mlynek, A. Peters, S. Schiller: Opt. Lett. **26**, 1430 (2001)
36 C. Gmachl, F. Capasso, R. Kohler, A. Tredicucci, A.L. Hutchinson, D.I. Sivco, J.N. Baillargeon, A.Y. Cho: IEEE Circuits and Devices **16**, 10 (2000); F. Capasso, R. Colombelli, R. Paiella, C. Gmachl, A. Tredicucci, D.I. Sivco, A.Y. Cho: Optics & Photonics News, **12**(5), 40 (2001)
37 B.A. Paldus, C.C. Harb, T.G. Spence, R.N. Zare, C. Gmachl, F. Capasso, D.I. Sivco, J.N. Baillargeon, A.L. Hutchinson, A.Y. Cho: Opt. Lett. **25**, 666 (2000)
38 K.P. Petrov, A.P. Roth, T.L. Patterson, T.P.S. Thoms, L. Huang, A.T. Ryan, D.J. Bamford: Appl. Phys. B: Lasers Opt. **70**, 777 (2000)
39 D. Richter, D.G. Lancaster, R.F. Curl, W. Neu, F.K. Tittel: Appl. Phys. B: Lasers Opt. **67**, 347 (1998); F.K. Tittel, D.G. Lancaster, D. Richter: Laser Phys. **10**, 348 (2000)
40 L.A. Eyres, P.J. Tourreau, T.J. Pinguet, C.B. Ebert, J.S. Harris, M.M. Fejer, L. Becouam, B. Gerard, E. Lallier: Appl. Phys. Lett. **79**, 904 (2001)
41 A. Garnache, A.A. Kachanov, F. Stoeckel, R. Houdré: J. Opt. Soc. Am. B **17**, 1589 (2000)
42 K.L. Vodopyanov: Laser Focus World, **37**, 225 (2001); Y. He, P. Wang, R.T. White, B.J. Orr: Optics & Photonics News, **13**(5), 56 (2002)
43 A.S.C. Cheung, T. Ma, H. Chen: Chem. Phys. Lett. **353**, 275 (2002)
44 A. O'Keefe: Chem. Phys. Lett. **293**, 331 (1998); A. O'Keefe, J.J. Scherer, J.B. Paul: Chem. Phys. Lett. **307**, 343 (1999); J.B. Paul, L. Lapson, J.G. Anderson: Appl. Opt. **40**, 4904 (2001)